2025 SCEC REPORT

GNSS and InSAR Integration for 3-D Deformation Field and Time Series in California

Zheng-Kang Shen
Department of Earth, Planetary, and Space Sciences, UCLA
Zhen Liu
Jet Propulsion Laboratory, NASA

We have developed a method to integrate GNSS and InSAR data to produce a 3-D surface velocity field of the Earth [Shen and Liu, 2025]. We have further applied this method to integrate GNSS and InSAR data for studying 3-D crustal deformation in California and western Nevada [Shen and Liu, 2025]. We also extended the approach to incorporate UAVSAR data, enabling an integrated solution for crustal deformation with a particular focus on estimating creep rates along faults that exhibit interseismic creep. We used the method to map the 3-D deformation field along the San Andreas fault in central California. Our preliminary result reveals both along-strike and vertical components of creep along the fault, which are continuous and distributed within a ~1-km-wide fault zone.

1. GNSS-InSAR velocity integration

We have developed a method to integrate GNSS and InSAR data to produce a 3-D velocity field. Key elements of the method include: (a) It adopts an optimized approach to interpolate discrete GNSS velocity data points into a continuous velocity field. (b) It takes a pragmatic approach to evaluate uncertainties for InSAR and GNSS measurements as well as interpolated GNSS velocities, to be used as weights for data input. (c) The ramp parameters of multiple tracks of InSAR data are solved through global optimization to minimize systematic biases in the solution. (d) InSAR LOS data are averaged within small grids, and de-ramped InSAR data and interpolated GNSS data are aggregated to solve for 3-D deformation in the grids through least-squares regression.

We applied the method to integrate GNSS and InSAR data to solve for 3-D crustal deformation of California and western Nevada. Up to three decades of GNSS data are incorporated, observed in both continuous and campaign modes, and combined with InSAR data acquired over a comparable time span using various satellites and sensors. The spatial-temporal coverage of InSAR data vary over the years, from limited spatial coverage of the ERS/Envisat satellite observations in southern California in 1990s-2010s to the Sentinel-1 and ALOS-2 observations that cover the entire study region from 2014 to the present. The deformation field is well resolved for most of the region, with horizontal component uncertainties averaging around 1 mm/yr or less and vertical uncertainties

about 2-3 mm/yr or less, effectively capturing both fault-related tectonic motions and more distributed deformation patterns across the region (Figure 1). The work has been published in Journal of Geophysical Research-Solid Earth [Shen and Liu, 2025].

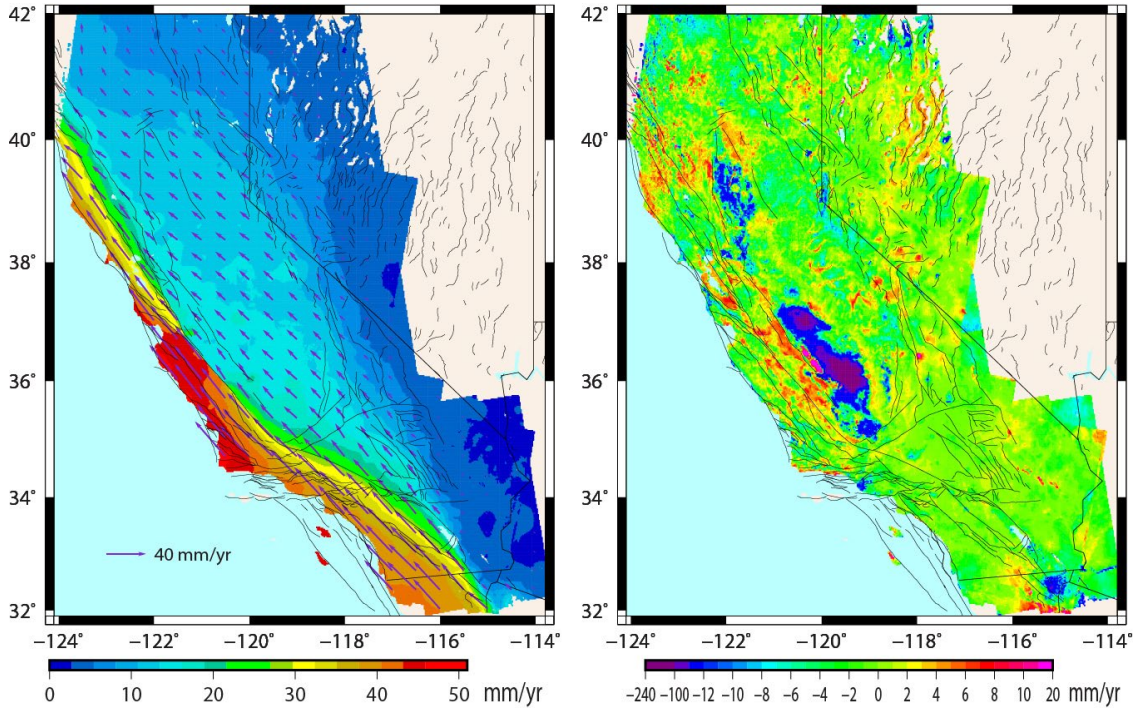

Figure 1. GNSS and InSAR derived 3-D crustal deformation in California and western Nevada. The left and right panels show horizontal and vertical velocity fields, revealing detailed deformation patterns associated with tectonic and non-tectonic (including hydrological) processes.

2. **GNSS/InSAR/UAVSAR Integration**

Since 2009, NASA's airborne UAVSAR program has been systematically mapping the entire San Andreas Fault (SAF) system. UAVSAR's optimized viewing geometry and very high spatial resolution make it possible to capture near-fault deformation with exceptional accuracy. Our time series analysis of UAVSAR data from the central SAF reveals localized deformation associated with fault creep, resolving spatial variations along strike at a resolution of ~6 m. We are expanding our analysis to include UAVSAR stacks along the SAF, particularly over known creeping fault segments. We processed the UAVSAR data using the JPL/Caltech InSAR Scientific Computing Environment (ISCE) software (https://github.com/isce-framework/isce2) [Rosen et al., 2012]. The resulting UAVSAR interferograms are then analyzed in a time series framework to estimate average line-of-sight rates and uncertainties, using an in-house variant of the Small Baseline Subset InSAR time series analysis approach [Liu et al., 2019; Shen and Liu, 2020, 2025]. The UAVSAR

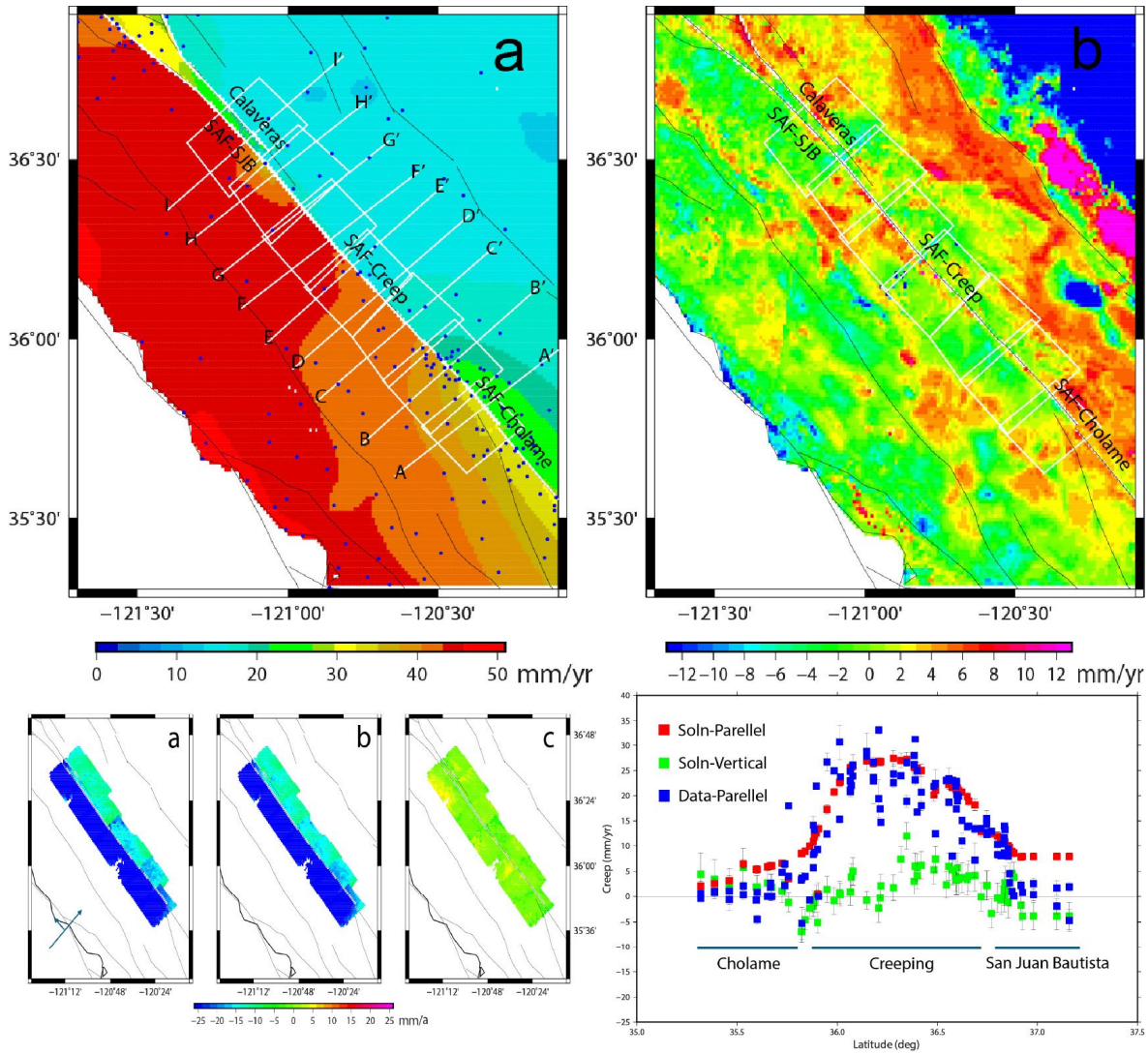

Figure 2. Joint solution of 3-D crustal deformation using integrated datasets of GNSS, InSAR, and UAVSAR. Upper: (a) and (b) are the solution for the horizontal amplitude and vertical components respectively. The blue dots mark the locations of GNSS sites. The white frames mark the surface imprints of the UAVSAR lines, from southeast to northwest are the 05008, 05010, 05012, 05014, 05016, 05018, and 05020 lines, respectively. The white lines denote locations of velocity profiles across the SAF. **Lower left:** (a), (b), and (c) are the UAVSAR de-ramped line-of-sight rate data, model predictions, and data postfit residuals. The two arrows in (a) show the vehicle flying direction and look direction respectively. **Lower right:** Solution of fault surface creep along SAF in central California. The red and green symbols denote the modeled along-strike and vertical components, and the blue symbol denotes the observed fault-parallel component of creep from a composite dataset (Johnson et al., 2022).

data are treated in a manner consistent with other InSAR datasets, removing orbital ramps

using GNSS constraints, and jointly analyzed with GNSS and InSAR data to generate the integrated 3-D deformation field and fault creep rate estimates.

We analyzed UAVSAR data from seven flight lines across the creep section of the SAF in central California over the period of 2009-2021. The UAVSAR data are integrated with the GNSS and InSAR data to derive 3-D velocity field in the Central SAF region shown in Figure 2. The region is divided into 0.01°×0.01°grid cells, and the solution is made through a least-squares regression for each cell. Our results show that:

a) The along-strike creep rates are of ~2–8 mm/yr, 10–26 mm/yr, and ~8 mm/yr across the Cholame, Creeping, and San Juan Bautista sections of the SAF, respectively. Vertical deformation shows a systematic pattern, with ~0–5 mm/yr uplift of the west side relative to the east side along the creeping section.
b) The creep pattern we derive is smooth and continuous along the fault. The inferred on-fault creep rates are on average higher than previous measurements obtained using creepmeters and InSAR, particularly for regions outside the main creeping section: ~2–8 mm/yr vs 0–5 mm/yr across Cholame, and ~8 mm/yr vs. ~2 mm/yr across San Juan Bautista.
c) These discrepancies suggest that (a) our results represent a regional, shallow depth-averaged creep pattern rather than localized point measurements at the surface, and (b) creep is distributed with ~20–75% of the deformation occurring within a ~1-km-wide fault zone.

3. GNSS-InSAR Time Series Integration

We have been developing a method to integrate GNSS and InSAR time series, and the corresponding software development is currently in progress. The overall workflow of the integration is illustrated in Figure 3. Tasks marked with check marks have been completed, while the remaining components are still under development.

References

Liu, Z., P.W. Liu, E. Massoud, T. G. Farr, P. Lundgren, J. S. Famiglietti (2019). Monitoring Groundwater Change in California's Central Valley Using Sentinel-1 and GRACE Observations, Geosciences, 9, 436; doi:10.3390/geosciences9100436.

Johnson, K. M., Murray, J. R., & Wespestad, C. (2022). Creep rate models for the 2023 US National Seismic Hazard Model: Physically constrained inversions for the distribution of creep on California faults. *Seismological Society of America*, *93*(6), 3151-3169.

Rosen, P. A., Gurrola, E., Sacco, G. F., & Zebker, H. (2012, April). The InSAR scientific computing environment. In *EUSAR 2012; 9th European conference on synthetic aperture radar* (pp. 730-733). VDE.

Shen, Z.-K., and Z. Liu (2020). Integration of GPS and InSAR Data for Resolving 3-Dimensional Crustal Deformation. *Earth and Space Science*, 7(4), e2019EA001036.

Shen, Z.-K., and Z. Liu (2025). GNSS and InSAR integration for 3-D crustal deformation in California and western Nevada, J. Geophys. Res., Nov;130(11):e2024JB030888.

Figure 3. GNSS-InSAR Time Series Integration Workflow